

RESEARCH ARTICLE

CORONAVIRUS

Broadly neutralizing antibodies target the coronavirus fusion peptide

Cherrelle Dacon^{1†}, Courtney Tucker^{1,2†}, Linghang Peng^{3†}, Chang-Chun D. Lee^{4†}, Ting-Hui Lin⁴, Meng Yuan⁴, Yu Cong⁵, Lingshu Wang⁶, Lauren Purser¹, Jazmean K. Williams⁷, Chul-Woo Pyo⁸, Ivan Kosik⁹, Zhe Hu⁹, Ming Zhao¹⁰, Divya Mohan¹, Andrew J. R. Cooper¹, Mary Peterson¹¹, Jeff Skinner¹¹, Saurabh Dixit⁵, Erin Kollins⁵, Louis Huzella⁵, Donna Perry⁵, Russell Byrum⁵, Sanae Lembirik⁵, David Drawbaugh⁵, Brett Eaton⁵, Yi Zhang⁶, Eun Sung Yang⁶, Man Chen⁶, Kwanyee Leung⁶, Rona S. Weinberg¹², Amarendra Pegu⁶, Daniel E. Geraghty⁸, Edgar Davidson⁷, Iyadh Douagi¹³, Susan Moir¹⁴, Jonathan W. Yewdell⁹, Connie Schmaljohn⁵, Peter D. Crompton¹¹, Michael R. Holbrook⁵, David Nemazee³, John R. Mascola⁶, Ian A. Wilson^{4,15}, Joshua Tan^{1*}

The potential for future coronavirus outbreaks highlights the need to broadly target this group of pathogens. We used an epitope-agnostic approach to identify six monoclonal antibodies that bind to spike proteins from all seven human-infecting coronaviruses. All six antibodies target the conserved fusion peptide region adjacent to the S2' cleavage site. COV44-62 and COV44-79 broadly neutralize alpha- and betacoronaviruses, including severe acute respiratory syndrome coronavirus 2 (SARS-CoV-2) Omicron subvariants BA.2 and BA.4/5, albeit with lower potency than receptor binding domain-specific antibodies. In crystal structures of COV44-62 and COV44-79 antigen-binding fragments with the SARS-CoV-2 fusion peptide, the fusion peptide epitope adopts a helical structure and includes the arginine residue at the S2' cleavage site. COV44-79 limited disease caused by SARS-CoV-2 in a Syrian hamster model. These findings highlight the fusion peptide as a candidate epitope for next-generation coronavirus vaccine development.

Coronaviruses consist of four genera that infect birds and mammals (1). Seven coronaviruses are known to cause human disease: the alphacoronaviruses HCoV-229E (human coronavirus 229E) and HCoV-NL63 (human coronavirus NL63), as well as the betacoronaviruses HCoV-OC43 (human coronavirus OC43), HCoV-HKU1 (human coronavirus HKU1), SARS-CoV (severe acute respiratory syndrome coronavirus), MERS-CoV (Middle East respiratory syndrome coronavirus), and SARS-CoV-2 (severe acute respiratory syndrome coronavirus 2). Whereas the first four coronaviruses generally cause mild disease, the latter three have brought about serious outbreaks in recent years. In particular, the ongoing COVID-19 pandemic caused by SARS-CoV-2 has resulted in more than 6 million deaths since the first cases were identified in 2019 (2). The currently dominant SARS-CoV-2 Omicron BA.2, BA.2.12.1, BA.4, and BA.5 subvariants are at

least partially resistant to most available vaccines and antibody therapeutics (3–6). Furthermore, two coronaviruses previously linked only to animal infection were recently detected in individuals with flu-like symptoms (7, 8). These developments highlight the importance of targeting conserved and functionally essential sites on coronaviruses.

Coronavirus infection is a multistep process that involves enzymatic cleavage and rearrangement of the surface spike protein (9). The SARS-CoV-2 spike contains two cleavage sites: a furin cleavage site at the boundary of the S1 and S2 subunits, and an S2' site that is conserved in coronaviruses. The spike protein is thought to be cleaved at the S1-S2 site during virus assembly, leaving the S1 and S2 subunits non-covalently linked. During entry, the SARS-CoV-2 spike protein uses the receptor binding domain (RBD) on the S1 subunit to engage angiotensin-converting enzyme 2 (ACE2) on target cells. After receptor binding, the S1 subunit is shed

and the S2' site is cleaved by the membrane enzyme transmembrane serine protease 2 (TMPRSS2) or endosomal cathepsins (1), leading to insertion of the fusion peptide into the cell membrane and viral fusion.

Much of the protection provided by COVID-19 vaccines arises from neutralizing antibodies that target the RBD (10). Likewise, all currently available therapeutic monoclonal antibodies (mAbs) target this domain (3). However, spike elements that participate in the subsequent stages of infection involve the more complex S2 fusion machinery with many moving parts, and these elements are more conserved than the RBD, which so far has been capable of retaining or even increasing binding to ACE2 despite a variety of mutations (11). Therefore, these sites are worth exploring as targets for novel COVID-19 vaccines and therapeutics that retain efficacy against new variants and protect against a wider range of coronaviruses. Progress in this direction has started with recent studies identifying several mAbs that target the conserved stem helix (12–16) and using unbiased approaches to screen for mAbs of interest (17–20). In this study, we carried out a large-scale survey of the binding landscape of broadly reactive mAbs against coronaviruses.

Identification of broadly reactive mAbs from COVID-19-convalescent donors

To identify individuals who are likely to harbor B cells that produce broadly reactive mAbs, we used a multiplex bead-based assay to examine plasma samples of 142 donors from a previously described cohort of COVID-19-convalescent individuals (20). We assessed plasma immunoglobulin G (IgG) reactivity toward spike glycoproteins of the seven human coronaviruses: SARS-CoV-2 (Wuhan-Hu-1 strain), SARS-CoV, MERS-CoV, HCoV-HKU1, HCoV-OC43, HCoV-NL63, and HCoV-229E. Nineteen donors were selected for mAb isolation and characterization on the basis of plasma IgG reactivity to the spike proteins of SARS-CoV-2 and at least two other betacoronaviruses (fig. S1A).

We next investigated human IgG⁺ memory B cells (MBCs) from the selected donors by using a two-stage screen to prioritize isolating mAbs with the greatest possible breadth of reactivity. First, we screened supernatants from 673,671 stimulated IgG⁺ B cells for binding

¹Antibody Biology Unit, Laboratory of Immunogenetics, National Institute of Allergy and Infectious Diseases, National Institutes of Health, Rockville, MD 20852, USA. ²Department of Biology, The Catholic University of America, Washington, DC 20064, USA. ³Department of Immunology and Microbiology, The Scripps Research Institute, La Jolla, CA 92037, USA. ⁴Department of Integrative Structural and Computational Biology, The Scripps Research Institute, La Jolla, CA 92037, USA. ⁵Integrated Research Facility, Division of Clinical Research, National Institute of Allergy and Infectious Diseases, National Institutes of Health, Frederick, MD 21702, USA. ⁶Vaccine Research Center, National Institute of Allergy and Infectious Diseases, National Institutes of Health, Bethesda, MD 20892, USA. ⁷Integral Molecular, Philadelphia, PA 19104, USA. ⁸Clinical Research Division, Fred Hutchinson Cancer Research Center, Seattle, WA 98109, USA. ⁹Cellular Biology Section, Laboratory of Viral Diseases, National Institute of Allergy and Infectious Diseases, National Institutes of Health, Bethesda, MD 20892, USA. ¹⁰Protein Chemistry Section, Research Technologies Branch, National Institute of Allergy and Infectious Diseases, National Institutes of Health, Rockville, MD 20852, USA. ¹¹Malaria Infection Biology and Immunity Section, Laboratory of Immunogenetics, National Institute of Allergy and Infectious Diseases, National Institutes of Health, Rockville, MD 20852, USA. ¹²New York Blood Center, Lindsley F. Kimball Research Institute, New York, NY 10065, USA. ¹³Flow Cytometry Section, Research Technologies Branch, National Institute of Allergy and Infectious Diseases, National Institutes of Health, Bethesda, MD 20892, USA. ¹⁴B Cell Immunology Section, Laboratory of Immunoregulation, National Institute of Allergy and Infectious Diseases, National Institutes of Health, Bethesda, MD 20892, USA. ¹⁵The Skaggs Institute for Chemical Biology, The Scripps Research Institute, La Jolla, CA 92037, USA.

*Corresponding author. Email: tanj4@nih.gov

†These authors contributed equally to this work.

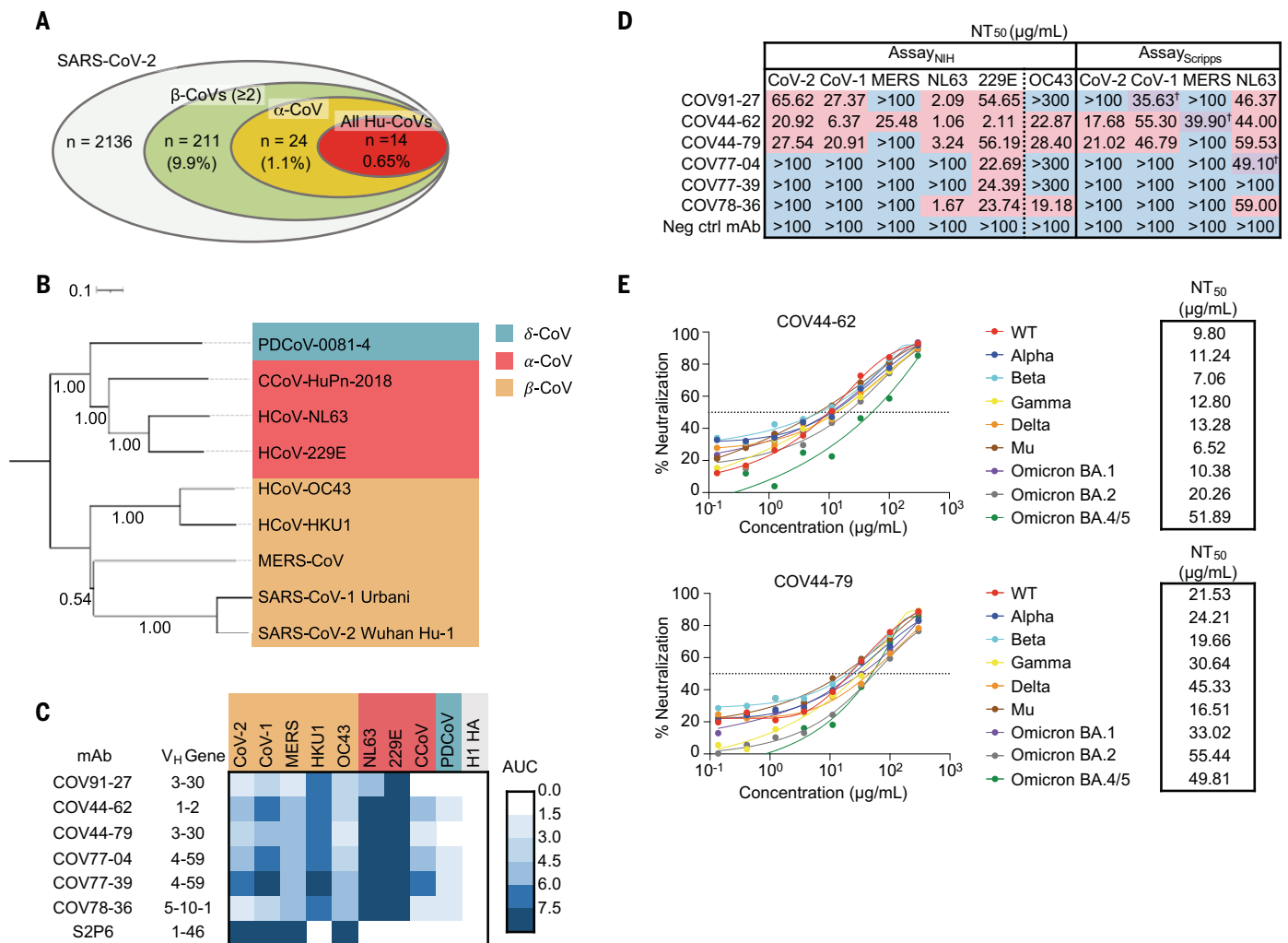


Fig. 1. Broadly neutralizing antibodies target coronaviruses associated with human disease. (A) Analysis of the frequency of MBCs expressing broadly reactive antibodies from 19 donors. Values in parentheses represent the percentage of SARS-CoV-2-reactive supernatants that also bind the specified subsets of nonsarbecovirus coronavirus spikes. A total of 10,356 MBC culture supernatants (50 to 100 B cells per well) were screened. *n*, number of MBC culture wells. (B) Phylogenetic relationships across the coronavirus spike proteins targeted by the broadly reactive mAbs were inferred by the neighbor-joining method in MEGA11 using full-length amino acid sequences of CoV spike proteins. Branch lengths are drawn to scale, and bootstrap values from 500 samplings are shown on the branches. The scale bar represents the number of amino acid substitutions per site. (C) Heatmap representing the binding of broadly reactive mAbs to spike proteins from coronaviruses across the *alpha*-, *beta*-, and *deltacoronavirus* genera. H1 hemagglutinin was included as a negative

control for mAb binding experiments, and area under the curve (AUC) values for each antigen are shown after subtraction with values for the negative control antigen CD4. (D) Values represent antibody titer at 50% neutralization (NT₅₀) against SARS-CoV-2 (Wuhan-Hu-1 strain), SARS-CoV (indicated as “CoV-1” in the figure), MERS-CoV, HCoV-NL63, and HCoV-229E envelope-pseudotyped lentivirus, as well as authentic HCoV-OC43. For Assay_{Scripps}, values are average of two experiments. For values with the † symbol, one NT₅₀ was determinable and one was not (i.e., >100 $\mu\text{g/mL}$), and the determinable NT₅₀ is shown. Negative control mAbs were anti-CoV-2 RBD CV503 (for OC43 assay) (20), anti-influenza HA CR9114 (for Assay_{NIH} except OC43) (42), and anti-dengue DEN3 (for Assay_{Scripps}) (43). NT₅₀ values were calculated using the dose-response-inhibition model with five-parameter Hill slope equation in GraphPad Prism 9. (E) Neutralization of SARS-CoV-2 variants of concern (pseudovirus, Assay_{Scripps}) by COV44-62 and COV44-79.

to the coronavirus spike panel used in the plasma screen. Supernatants from only 2% ($n = 211$) of the MBC culture wells met our criteria for broad reactivity by binding to at least three betacoronavirus spike proteins (Fig. 1A). Next, we developed an optofluidics assay to isolate individual MBCs of interest using the Berkeley Lights Beacon system (fig. S1B). Candidate MBCs identified in the supernatant screen were sorted individually

into nanoliter-volume pens and assessed in real time for secretion of mAbs that bound to beads coated with a cocktail of MERS-CoV and HCoV-OC43 spikes, followed by beads coated with SARS-CoV-2 spike. Double-positive MBCs were exported for single-cell reverse transcription polymerase chain reaction and antibody expression as recombinant IgG1. In total, we obtained 60 IgG mAbs with reactivity to at least three coronaviruses.

To fully examine their breadth, we tested the 60 mAbs for binding to spikes from the seven human coronaviruses. Only six mAbs—COV91-27, COV44-62, COV44-79, COV77-04, COV77-39, and COV78-36—bound to spike proteins from all seven coronaviruses (Fig. 1, B and C). Notably, four of the six also bound to spike from two new coronaviruses that have recently been associated with human disease: canine CoV HuPn-2018 (CCoV-HuPn-2018) and

porcine deltacoronavirus 0081-4 (PDCoV-0081-4) (7, 8) (Fig. 1C). The six broadly reactive mAbs were isolated from four different donors and were encoded by four different heavy-chain variable (VH) genes (VH1-2, VH3-30, VH4-59, and VH5-10-1) (table S1). Five mAbs were highly mutated, with VH nucleotide mutation frequencies ranging from 10 to 13% (fig. S1C). Given that these mAbs were isolated from COVID-19-convalescent individuals in New York ~1 month after the first outbreak in March 2020, these mutation levels suggest that the B cells were primed during an earlier seasonal coronavirus infection and possibly reactivated during SARS-CoV-2 infection.

COV44-62 and COV44-79 broadly neutralize coronaviruses

We assessed the neutralizing potency of the six mAbs against SARS-CoV-2, SARS-CoV, MERS-CoV, HCoV-NL63, and HCoV-229E envelope pseudotyped viruses, as well as authentic HCoV-OC43. COV44-62 and COV44-79 showed the broadest functional reactivity, neutralizing the betacoronaviruses SARS-CoV-2, SARS-CoV, and HCoV-OC43, as well as the alphacoronaviruses HCoV-NL63 and HCoV-229E (Fig. 1D and fig. S1D). Moreover, both mAbs neutralized SARS-CoV-2 variants of concern, including the Omicron BA.2 and BA.4/5 sub-variants, as well as authentic SARS-CoV-2

(Fig. 1E and fig. S1E). COV44-62 also neutralized MERS-CoV, whereas no other mAbs neutralized this virus within the concentrations tested.

Broadly reactive mAbs target the coronavirus fusion peptide

To determine the domain of SARS-CoV-2 spike that was targeted by the six broadly reactive mAbs, we assessed mAb binding to the SARS-CoV-2 S2 subunit as well as the RBD and N-terminal domain (NTD) of the S1 subunit. All six mAbs bound only to the S2 subunit (Fig. 2A). VJ germline-reverted versions of the broadly neutralizing mAbs COV44-62 and COV44-79

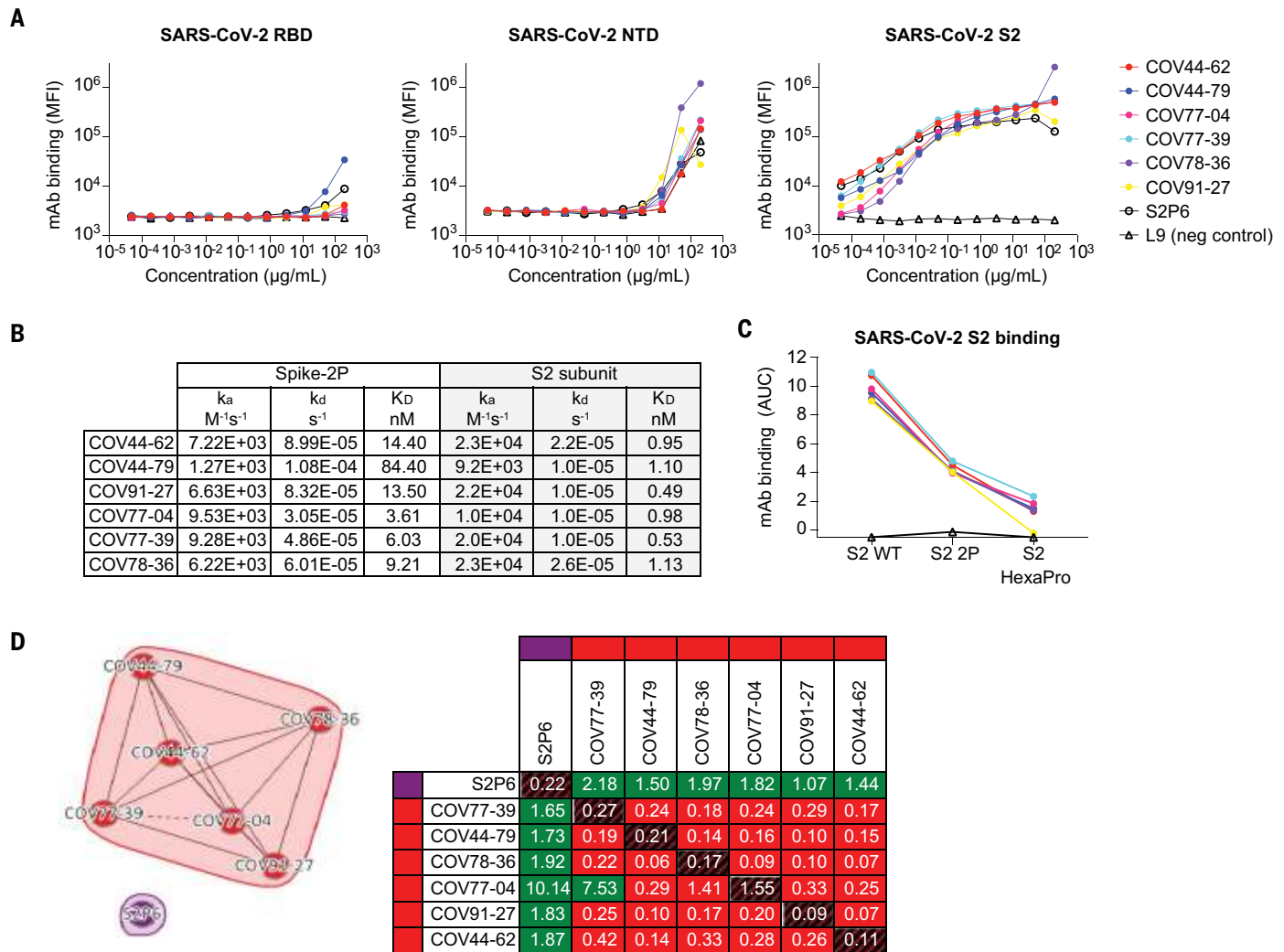


Fig. 2. Broadly reactive mAbs target the same region within the SARS-CoV-2 S2 subunit. (A) Titration curves for mAb binding to selected regions within the SARS-CoV-2 spike protein: the RBD, NTD, and S2 subunit. Interconnected data points are shown without curve fitting. L9 is a malaria-specific mAb used as a negative control (44). MFI, median fluorescence intensity. (B) On rates, off rates, and dissociation constants of the six fusion peptide Fabs for binding to SARS-CoV-2 prefusion-stabilized spike (2P) with an unmodified furin cleavage site and the nonstabilized S2 subunit. k_a , association rate constant; k_d , dissociation rate constant;

K_D , equilibrium dissociation constant. (C) Fusion peptide mAb binding (AUC) to wild-type (WT) SARS-CoV-2 S2 subunit and S2 subunit constructs modified with two (2P) or six (HexaPro) stabilizing proline mutations. (D) Epitope binning of broadly reactive antibodies versus the S2 stem-helix targeting mAb S2P6. All included antibodies were tested as both ligands and analytes. Solid lines indicate two-way competition, whereas the dashed line indicates one-way competition. Red boxes indicate competing antibody pairs, green boxes indicate noncompeting antibody pairs, and hatched boxes indicate self-competition.

showed weaker binding to S2 than the mutated versions (fig. S2A), suggesting that somatic mutations were important for improving binding to the target site. A surface plasmon resonance (SPR) kinetics assay determined the binding affinity of antigen-binding fragments (Fabs) derived from these mAbs for prefusion-stabilized whole SARS-CoV-2 spike (2P, with an intact S1-S2 cleavage site) and the unmodified S2 subunit. The Fabs bound with low-to-moderate nanomolar affinity to both proteins, but their affinity for the S2 subunit was 3- to 76-fold higher than their affinity for whole spike (Fig. 2B and fig. S2B). There were no substantial differences between the six Fabs in their affinity for the S2 subunit. The mAbs showed reduced binding to a form of S2 that had been stabilized with two proline mutations (S2-2P) and bound more poorly still to a further stabilized version with six proline mutations (S2-HexaPro) (Fig. 2C). SPR-based competition showed that the six mAbs competed for the same binding site on the S2 subunit (Fig. 2D), but none competed with S2P6, a control mAb targeting the stem helix region (I2), indicating their specificity for a distinct site on S2.

To further investigate the specificity of these mAbs, we performed SPR-based peptide mapping using an array of 15-amino acid (15-mer) overlapping peptides that spanned the entire SARS-CoV-2 S2 subunit (S686 to K1211, accession no. YP_009724390.1). All six mAbs bound to peptides 42 to 44, which share the $_{815}\text{RSFIEDLLF}_{823}$ motif (Fig. 3A). This motif is located within the SARS-CoV-2 fusion peptide region, directly C-terminal to the S2' cleavage site. To determine the diversity of this region across coronaviruses, we selected 34 viral isolates representing each of the four coronavirus genera (Fig. 3B). Nearly all amino acid positions in the $_{815}\text{RSFIEDLLF}_{823}$ motif were conserved in >85% of viruses selected; the exception was F₈₁₇, which was conserved in <50% of isolates examined (Fig. 3, B and C). The fusion peptide appears partially surface-exposed in a range of coronavirus spike proteins, including those of SARS-CoV-2, SARS-CoV, MERS-CoV, and MHV (mouse hepatitis virus) (21, 22) (Fig. 3C and fig. S3A). However, antibody access to this site may be partially occluded by the S1 subunit on an adjacent protomer, consistent with stronger binding to the S2 subunit relative to the SARS-CoV-2 spike (Fig. 2B and fig. S3B).

The mAb specificity toward the fusion peptide is consistent with their reduced binding to the HexaPro S2 construct (Fig. 2C), which includes a nonconservative F817P mutation at this site (23). To identify key amino acids for mAb binding, we performed an alanine scan on a peptide encompassing residues 810 to 830 and focused on residues targeted by the broadly neutralizing mAbs COV44-62 and

COV44-79 (Fig. 3D). Four amino acids—E819, D820, L822, and F823—were important for binding of COV44-62, where mutation of the F823 residue abolished binding. Similarly, residues critical for the binding of COV44-79 were E819, D820, and F823 but also included R815 at the S2' cleavage site (Fig. 3D). All five residues identified as important for COV44-62 or COV44-79 binding are among the most conserved residues in the coronavirus spike protein. D820 and L822 are completely conserved, whereas R815, E819, and F823 are conserved in 33 of 34 coronaviruses (Fig. 3, B and E). Amino acid mutations at the peptide level may have different effects from mutations in the intact spike protein, where modified interactions with surrounding residues may also affect antibody binding. Therefore, we screened the six mAbs using a shotgun alanine mutagenesis approach, whereby every amino acid in the S2 subunit of intact spike was individually mutated to generate a panel of spike mutants (Fig. 3F and fig. S3, C and D). In general, this assay identified a greater number of residues as important for mAb binding, including some with a more intermediate phenotype. For COV44-62, D820, L822, and F823 were again crucial for binding, and K825, D830, and R815 were also identified as important (Fig. 3F). For COV44-79, the results closely matched the peptide alanine scan, with the same four amino acids (R815, E819, D820, and F823) identified as the most critical. When the six mAbs were analyzed as a group, we found that only the four broadest neutralizing mAbs were negatively affected by the R815A mutation (fig. S4, A and B), suggesting that binding to the S2' cleavage site may be a distinguishing property of broadly neutralizing mAbs against this site.

Crystal structures of anti-fusion peptide antibodies

To elucidate the molecular characteristics of anti-fusion peptide antibodies that neutralize SARS-CoV-2, the Fabs of the three broadest neutralizing mAbs (COV44-62, COV44-79, and COV91-27) were complexed with 15-mer peptides containing the fusion peptide sequence (Fig. 4). Crystal structures were determined to 1.46-, 2.8-, and 2.3-Å resolution, respectively (Fig. 4, fig. S5, and table S2). Fourteen of the 15 peptide residues were visible in the electron density map for COV44-62 (fig. S5A), 13 of which have a buried surface area (BSA) >0 Å² in complex with antibody. For COV44-79, 12 of the 15 peptide residues were visible (fig. S5A), 10 of which have a BSA >0 Å². Similarly, in COV91-27, 12 peptide residues had interpretable density (Fig. 4C and fig. S5A), with nine exhibiting a BSA >0 Å². The fusion peptide forms a helix as in the prefusion state of the SARS-CoV-2 spike (fig. S5B). All three complementarity-determining regions (CDRs) of the heavy chain

(HC) of all three Fabs are involved in peptide recognition, whereas CDR1 and CDR3 of the light chain (LC) of COV44-62, and only LCDR3 of COV44-79 and COV91-27, contact the peptide (Fig. 4, A to C). The BSA on each Fab is dominated by the HC and is 791 Å² for COV44-62 (627 Å² by HC and 164 Å² by LC), 634 Å² for COV44-79 (505 Å² by HC and 129 Å² by LC), and 573 Å² for COV91-27 (447 Å² by HC and 126 Å² by LC). The fusion peptide makes side-chain and backbone H-bonds and salt bridges with COV44-62 mainly through K814, R815, E819, D820, L822, F823, and N824, and hydrophobic interactions through I818, L822, and F823 (Fig. 4D). These residues include the key residues (E819, D820, L822, and F823) identified by site-directed mutagenesis (Fig. 3D). The fusion peptide did not form as many interactions with COV44-79 and COV91-27 (Fig. 4, E and F). However, R815, E819, and D820 contributed H-bonds and salt bridges, and I818, L822, and F823 made hydrophobic interactions. In all three antibodies, R815, S816, I818, E819, D820, L822, and F823 contributed the most BSA to the interaction (Fig. 4, G to I). There was partial overlap between the residues of COV44-62 and COV44-79 that interacted with the fusion peptide and those that were mutated from the germline (fig. S6), consistent with the reduction in binding of germline-reverted versions of these mAbs (fig. S2A). The structural results are consistent with the peptide and spike protein mutagenesis data that identify the key binding residues (Fig. 3, D to F, and fig. S3D). Notably, the arginine at the S2' cleavage site is involved in recognition by these anti-fusion peptide antibodies. Although the antibodies all interact with one face of the fusion peptide helical structure (fig. S5D), their approach angles to the peptide differ. Superimposition of the fusion peptide structures onto an intact SARS-CoV-2 spike trimer structure in the prefusion state showed a potential clash with the S protein, suggesting that a conformational change or conformational dynamics around the fusion peptide is required to accommodate antibody targeting (fig. S5C). Nevertheless, these antibodies have neutralization activity against SARS-CoV-2 and therefore are able to interact with the fusion peptide on the virus (Fig. 1D).

Response to the fusion peptide after vaccination and infection

We compared the binding of polyclonal IgG from mRNA-1273-vaccinated donors (fig. S7A), COVID-19-convalescent individuals, and COVID-19-naïve individuals to the SARS-CoV-2 fusion peptide (peptide 43) (Fig. 3A and fig. S7B). All COVID-19-naïve donors showed minimal binding to the peptide, indicating a minor contribution by previous seasonal coronavirus infections to circulating fusion peptide-specific IgG. Although there was an increased response in

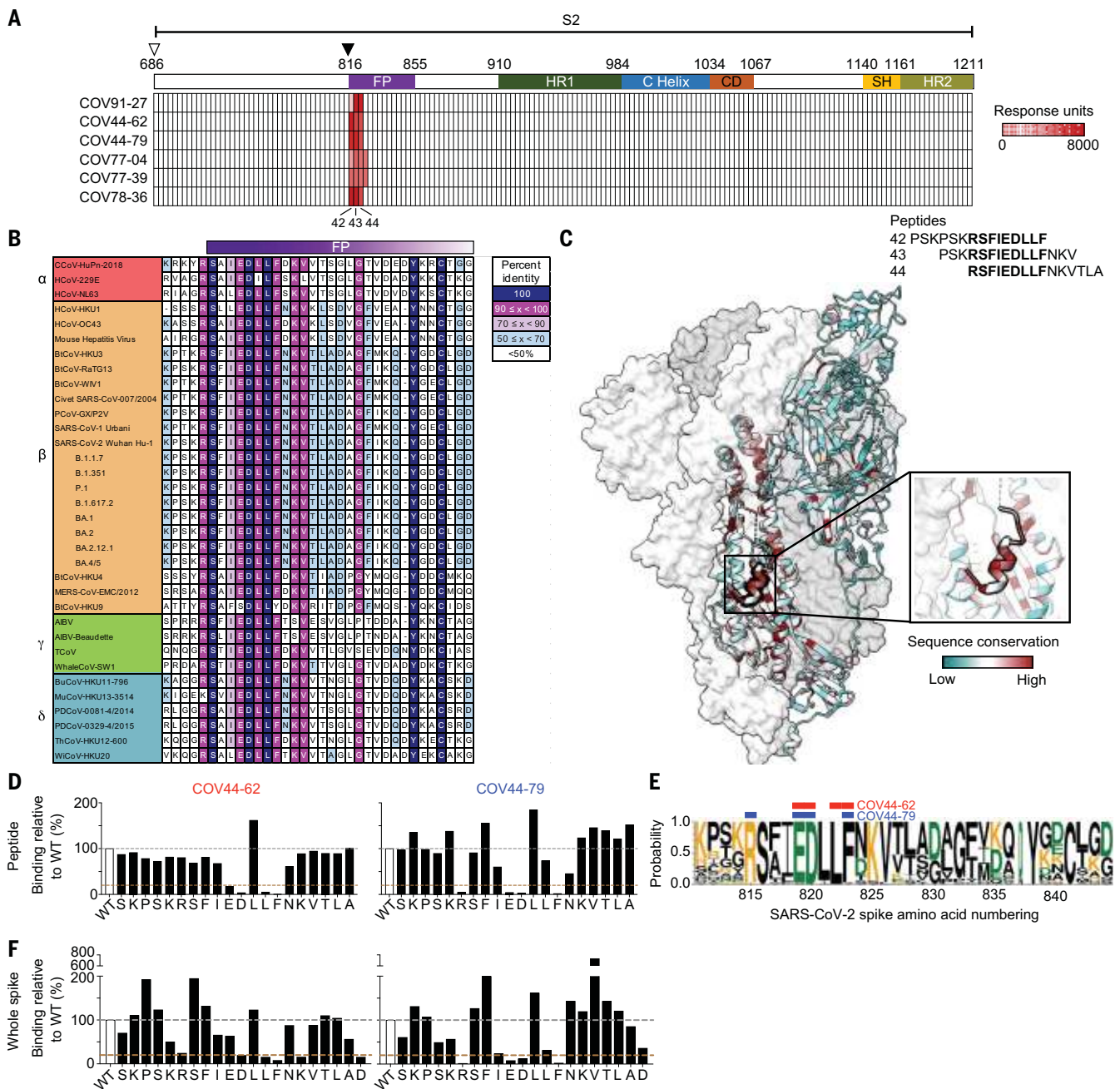


Fig. 3. Broadly neutralizing antibodies target the conserved fusion peptide. (A) Heatmap of SARS-CoV-2 S2 peptide array. Binding responses were assessed by SPR using a 15-mer peptide array with 12-amino acid overlap covering the entire S2 subunit. Each column within the map represents a single peptide. The white triangle denotes the S1-S2 cleavage site, and the black triangle indicates the S2' cleavage site. FP, fusion peptide; HR1, heptad repeat 1; C Helix, central helix; CD, connector domain; SH, stem helix; HR2, heptad repeat 2. (B) Sequence alignment of the fusion peptide from 34 viral isolates representing a diverse group of coronaviruses across four genera. This analysis was performed using MAFFT v7 with a BLOSUM62 scoring matrix and the L-INS-I algorithm. Single-letter abbreviations for amino acids: A, Ala; C, Cys; D, Asp; E, Glu; F, Phe; G, Gly; H, His; I, Ile; K, Lys; L, Leu; M, Met; N, Asn; P, Pro; Q, Gln; R, Arg; S, Ser; T, Thr; V, Val; W, Trp; and Y, Tyr. (C) Sequence conservation of prefusion SARS-CoV-2 spike protein (PDB ID 6VSB); the fusion peptide (amino acids 816 to 843) is outlined in black. The inset shows a magnified view of this region. (D) Alanine scan evaluating the

binding of COV44-62 and COV44-79 to the SARS-CoV-2 fusion peptide. Responses were normalized to the wild-type sequence. A cutoff of 20% (brown dashed line) was used to identify residues that were critical for binding. (E) Sequence logo plot of diversity within the fusion peptide region of coronaviruses from 34 isolates, built using WebLogo 3. Letter height is proportional to the probability of an amino acid at a given position, and amino acid residues are colored by charge. Narrow stacks (amino acids) indicate deletions or gaps in the sequences. Numbering is based on the SARS-CoV-2 Wuhan-Hu-1 sequence. The key residues in the epitope footprints of mAbs COV44-62 (red) and COV44-79 (blue), based on peptide alanine scanning, are highlighted above the logo plot. (F) Amino acids critical for the binding of COV44-62 and COV44-79, identified by shotgun alanine mutagenesis of S2 residues on whole spike protein. Only fusion peptide residues are shown. Key residues were identified on the basis of a <20% signal relative to wild-type spike (brown dashed line), with no corresponding loss of signal for a control mAb, which targets the spike protein but does not bind to this site (fig. S3C).

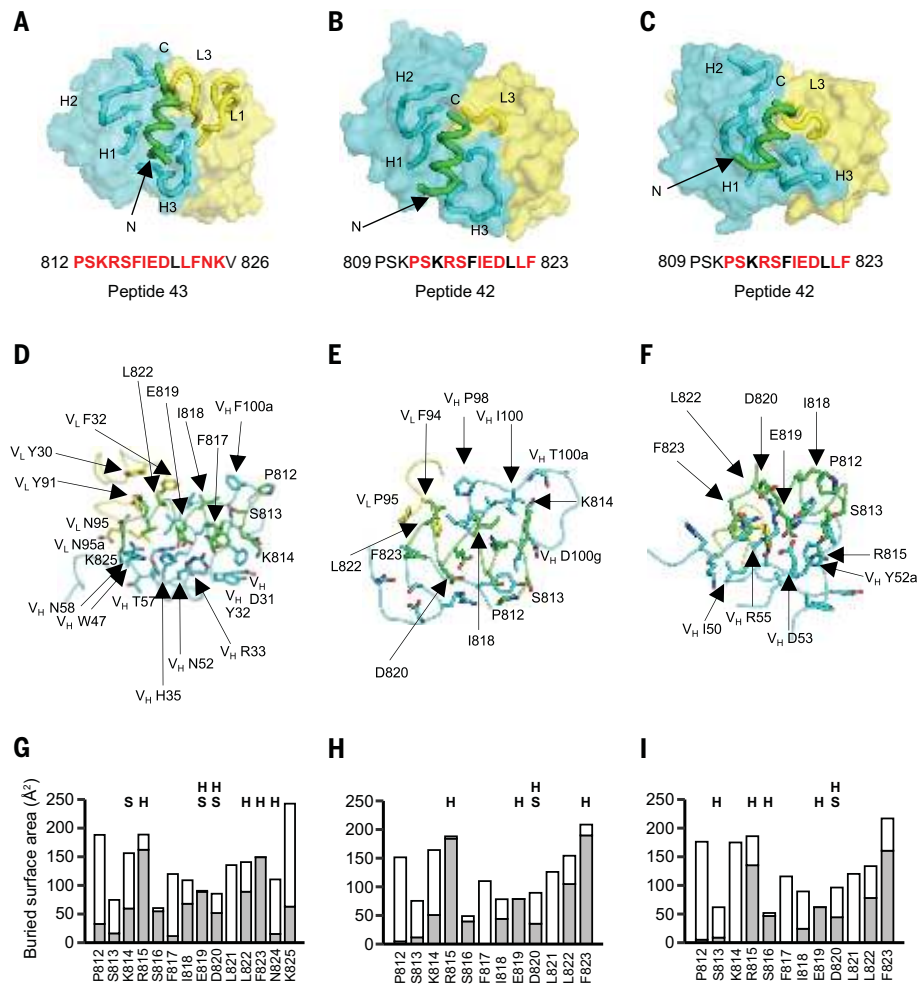


Fig. 4. Crystal structures of COV44-62, COV44-79, and COV91-27 in complex with SARS-CoV-2 fusion peptide. (A to C) Overall interactions of (A) COV44-62, (B) COV44-79, and (C) COV91-27 with the fusion peptide. Fabs are shown in molecular surface representation, and the CDRs and peptides are represented as tubes. Cyan and yellow denote the heavy and light chains of the Fabs, respectively. Peptides are shown in green. H1, H2, H3, L1, and L3 denote CDRs in the heavy (H) and light (L) chains. The resolutions of the crystal structures are 1.46, 2.8, and 2.3 Å for the COV44-62, COV44-79, and COV91-27 complexes, respectively. Peptide residues observed in the crystal structures are in bold; residues that interact with antibodies (BSA >0 Å²) are in red. (D to F) Details of the interactions between (D) COV44-62, (E) COV44-79, and (F) COV91-27 with the fusion peptide. V_H and V_L indicate the variable domains of the heavy and light chains, respectively. Kabat numbering was used for the Fabs; numbering in the native spike protein was used for the fusion peptide. Colors for the heavy chain, light chain, and fusion peptide are as in (A). (G to I) BSA (gray) and accessible surface area (white) of each residue of the fusion peptide in complex with antibody are shown in the stacked bar chart. Residues that form polar interactions with COV44-62, COV44-79, and COV91-27 are denoted atop the corresponding bar with “H” for a hydrogen bond or “S” for a salt bridge. Buried and accessible surface areas were calculated with PISA (45).

several vaccine recipients after the second dose ($P = 0.025$), this was not enhanced by administration of a booster dose. The COVID-19-convalescent donors did not have significantly higher responses than vaccinated donors after the second dose ($P = 0.864$). However, several convalescent donors had the highest responses in all three cohorts, suggesting that SARS-CoV-2 infection triggers a strong fusion peptide-specific antibody response in some individuals.

COV44-62 and COV44-79 inhibit membrane fusion

Spike-mediated cell fusion relies on insertion of the fusion peptide into the target cell membrane and thus might be inhibited by antibody binding to the fusion peptide. Consistent with this, COV44-62 and COV44-79 inhibited the fusion of cells expressing SARS-CoV-2 spike and cells expressing the ACE2 receptor in an imaging-based assay (Fig. 5A). We further tested the six fusion peptide-specific mAbs

in a more quantitative assay wherein fusion would trigger the release of an enzyme that cleaves a chromogenic substrate. Only the mAbs that neutralized SARS-CoV-2 were able to strongly inhibit fusion (Fig. 5B).

COV44-79 limits disease in the Syrian hamster model

We evaluated the in vivo efficacy of COV44-62 and COV44-79 against SARS-CoV-2 infection in the Syrian hamster model, a well-established model that recapitulates features of moderate-to-severe COVID-19 in humans (24–26). We converted the Fc regions of the two mAbs to hamster IgG2 to allow optimal Fc function. The mAbs were administered intraperitoneally at 16 mg per kilogram of body weight (mg/kg), followed by intranasal administration of 5 log₁₀ plaque-forming units of SARS-CoV-2 WAI 24 hours later (Fig. 5, C and D, and fig. S8). Hamsters treated with COV44-79 and, to a lesser extent, COV44-62 had a smaller decrease in body weight and recovered more quickly than untreated hamsters ($P < 0.01$ from days 3 to 7 for COV44-79; $P < 0.05$ from days 5 to 7 for COV44-62) (Fig. 5C). Similar results were observed in a second experiment in which COV44-79 was tested in comparison with a hamster IgG2 isotype control (fig. S8B). Furthermore, semiquantitative scoring revealed that hamsters treated with COV44-79 had less interstitial pneumonia than untreated hamsters on day 7 ($P < 0.05$) (Fig. 5D). COV44-79 was also able to slightly reduce lung viral titers relative to control hamsters, on the basis of subgenomic RNA quantification and plaque assay analysis (fig. S8C).

Discussion

The broad conservation and functional importance of the fusion peptide highlight the potential of this site as a candidate for coronavirus vaccine development. These findings have parallels to studies of HIV-1 gp120, where the surface-exposed fusion peptide was identified as a target of neutralizing mAbs (27). This discovery led to the investigation of the HIV-1 fusion peptide as a candidate immunogen to elicit broadly neutralizing antibodies in animals (28); subsequent animal studies have increased the potency and breadth of the fusion peptide-targeting antibody response (29). Despite these potential advantages, the coronavirus fusion peptide has not been a major focus for development of therapeutic mAbs and COVID-19 vaccines. The main drawback of the mAbs described here is their comparatively low in vitro neutralization potency. These mAbs fit into a wider trend of a trade-off between potency and breadth: Highly potent mAbs that target the RBD are restricted to sarbecoviruses and most do not neutralize all variants of SARS-CoV-2 (3, 5, 6, 20, 30), whereas mAbs that target the stem helix (12–16) and

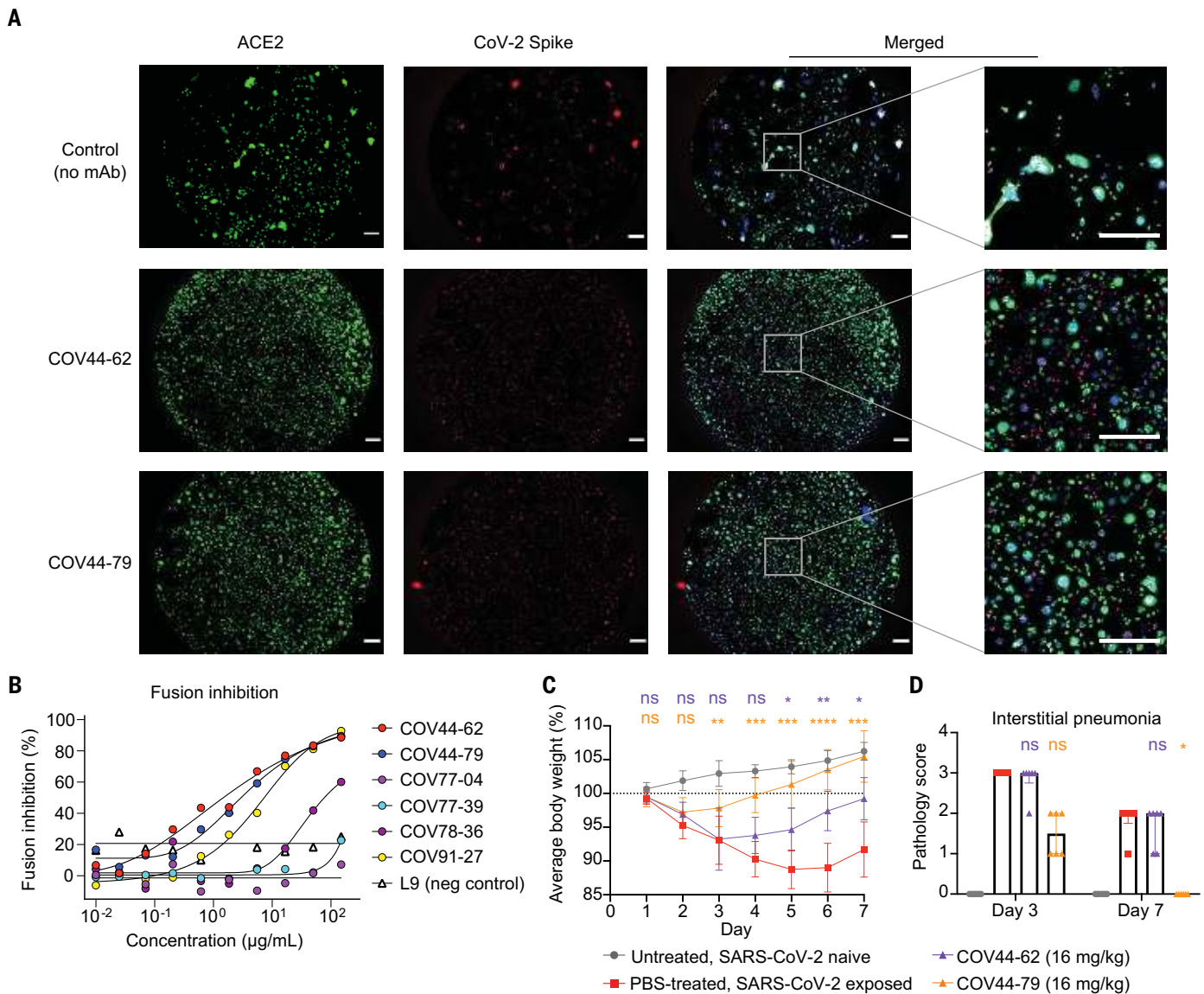


Fig. 5. COV44-62 and COV44-79 inhibit SARS-CoV-2 spike-mediated fusion and COV44-79 limits disease in a Syrian hamster model. (A) Images of fusion between HeLa cells stably expressing SARS-CoV-2 spike (red fluorescent protein) and HeLa cells stably expressing the ACE2 receptor (green fluorescent protein) after counterstaining with Hoechst (blue). Cells were cocultured in the presence of COV44-62 or COV44-79, or without a mAb (control). Scale bars, 500 μm . (B) Fusion inhibition of six fusion peptide-specific mAbs in a quantitative assay. (C) Weight change for SARS-CoV-2-naïve animals versus virus-exposed animals that were mock-treated or treated with 16 mg/kg of mAb. Statistical significance for average body weight was analyzed

across the 7-day time course using a mixed-effects repeated measures model with Dunnett's post-test multiple comparison ($n = 12$ animals from days 0 to 3; $n = 6$ animals from days 4 to 7). Error bars show mean \pm SD. (D) Pathology scores for SARS-CoV-2-naïve animals versus virus-exposed animals that were mock-treated or treated with 16 mg/kg of mAb. Scores for interstitial pneumonia pathology (days 3 and 7) based on gross pathology observations were statistically analyzed by a Kruskal-Wallis test with Dunn's post-test multiple comparison ($n = 6$ to 12 animals per condition) between the mAb-treated and mock-treated groups on each day. Bars show median and interquartile range. * $P < 0.05$; ** $P < 0.01$; *** $P < 0.001$; **** $P < 0.0001$; ns, not significant.

those identified here have greater breadth but are less potent. However, as previously reported for at least one antistem helix mAb (15), COV44-79 performed better than expected in the hamster model, which suggests that it may function in a way that is not captured effectively in the neutralization assay. For instance, Fc effector functions may enhance activity, as observed with anti-SARS-CoV-2 antibodies with other specificities (31–33).

Moreover, there is substantial scope for improvement for mAbs with this specificity, and subsequent studies may discover mAbs with higher potency, as with the HIV-1 fusion peptide (34). Techniques to improve antibody affinity and potency could also be useful (35, 36).

Additionally, vaccination with fusion peptide constructs may trigger a polyclonal response of greater magnitude and potency. We found that three doses of the mRNA-1273 vaccine did not

produce strong antibody responses to the fusion peptide, although several COVID-19-convalescent individuals exhibited strong antibody responses to this site. This observation is consistent with greater exposure of the S2 subunit to B cells during natural infection as a result of S1 uncoupling, which likely occurs less frequently with prefusion-stabilized spike protein. Furthermore, depletion of fusion peptide-specific antibodies from the serum

of COVID-19–convalescent patients resulted in a 20% reduction in SARS-CoV-2 neutralization (37), and reactivity to the fusion peptide was correlated with neutralization titer (38), indicating that polyclonal antibodies to the fusion peptide can play an appreciable role. Thus, our findings are consistent with previous studies that have highlighted the potential utility of the fusion peptide as a target epitope (37–41), and the fusion peptide–targeted mAbs provide additional tools to combat COVID-19 and enhance pandemic preparedness.

REFERENCES AND NOTES

- P. V'kovski, A. Kratzel, S. Steiner, H. Stalder, V. Thiel, *Nat. Rev. Microbiol.* **19**, 155–170 (2021).
- E. Dong, H. Du, L. Gardner, *Lancet Infect. Dis.* **20**, 533–534 (2020).
- S. Iketani *et al.*, *Nature* **604**, 553–556 (2022).
- N. Andrews *et al.*, *N. Engl. J. Med.* **386**, 1532–1546 (2022).
- E. Takashita *et al.*, *N. Engl. J. Med.* [10.1056/NEJMc2207519](https://doi.org/10.1056/NEJMc2207519) (2022).
- L. A. VanBlargan *et al.*, *Nat. Med.* **28**, 490–495 (2022).
- J. A. Lednický *et al.*, *Nature* **600**, 133–137 (2021).
- A. N. Vlasova *et al.*, *Clin. Infect. Dis.* **74**, 446–454 (2022).
- C. B. Jackson, M. Farzan, B. Chen, H. Choe, *Nat. Rev. Mol. Cell Biol.* **23**, 3–20 (2022).
- J. S. Tregoning, K. E. Flight, S. L. Higham, Z. Wang, B. F. Pierce, *Nat. Rev. Immunol.* **21**, 626–636 (2021).
- T. N. Starr *et al.*, *Cell* **182**, 1295–1310.e20 (2020).
- D. Pinto *et al.*, *Science* **373**, 1109–1116 (2021).
- M. M. Sauer *et al.*, *Nat. Struct. Mol. Biol.* **28**, 478–486 (2021).
- C. Wang *et al.*, *Nat. Commun.* **12**, 1715 (2021).
- P. Zhou *et al.*, *Sci. Transl. Med.* **14**, eab9215 (2022).
- W. Li *et al.*, *Cell Rep.* **38**, 110210 (2022).
- F. Amanat *et al.*, *Cell* **184**, 3936–3948.e10 (2021).
- K. A. Huang *et al.*, *PLOS Pathog.* **17**, e1009352 (2021).
- W. N. Voss *et al.*, *Science* **372**, 1108–1112 (2021).
- H. Cho *et al.*, *Sci. Transl. Med.* **13**, eabj5413 (2021).
- A. C. Walls *et al.*, *Nature* **531**, 114–117 (2016).
- Y. Yuan *et al.*, *Nat. Commun.* **8**, 15092 (2017).
- C. L. Hsieh *et al.*, *Science* **369**, 1501–1505 (2020).
- J. F. Chan *et al.*, *Clin. Infect. Dis.* **71**, 2428–2446 (2020).
- M. Imai *et al.*, *Proc. Natl. Acad. Sci. U.S.A.* **117**, 16587–16595 (2020).
- S. F. Sia *et al.*, *Nature* **583**, 834–838 (2020).
- R. Kong *et al.*, *Science* **352**, 828–833 (2016).
- K. Xu *et al.*, *Nat. Med.* **24**, 857–867 (2018).
- R. Kong *et al.*, *Cell* **178**, 567–584.e19 (2019).
- M. A. Tortorici *et al.*, *Nature* **597**, 103–108 (2021).
- I. Ullah *et al.*, *Immunity* **54**, 2143–2158.e15 (2021).
- R. Yamin *et al.*, *Nature* **599**, 465–470 (2021).
- Y. C. Bartsch *et al.*, *Nat. Med.* **27**, 454–462 (2021).
- C. H. Shen *et al.*, *Cell Host Microbe* **27**, 531–543.e6 (2020).
- S. Kratochvíl *et al.*, *Immunity* **54**, 2859–2876.e7 (2021).
- A. Wellner *et al.*, *Nat. Chem. Biol.* **17**, 1057–1064 (2021).
- C. M. Poh *et al.*, *Nat. Commun.* **11**, 2806 (2020).
- W. R. Morgenlander *et al.*, *J. Clin. Invest.* **131**, e146927 (2021).
- X. Sun *et al.*, *Nat. Microbiol.* **7**, 1063–1074 (2022).
- N. Vanderheijden *et al.*, *Front. Immunol.* **12**, 790415 (2022).
- D. L. N. F. Maeda *et al.*, *Proc. Natl. Acad. Sci. U.S.A.* **118**, e2025622118 (2021).
- C. Dreyfus *et al.*, *Science* **337**, 1343–1348 (2012).
- T. F. Rogers *et al.*, *Science* **369**, 956–963 (2020).
- L. T. Wang *et al.*, *Immunity* **53**, 733–744.e8 (2020).
- E. Krissinel, K. Henrick, *J. Mol. Biol.* **372**, 774–797 (2007).

ACKNOWLEDGMENTS

We thank the blood sample donors at the New York Blood Center; S. Bangaru, G. Ozorowski, A. Torrents de la Peña, and A. Ward for providing HCoV-OC43 and MERS-CoV; G. Wright and N. Muller-Sienert (Wright lab, University of York) for providing recombinant CD4; L. Wang and R. Seder for providing the L9 antibody; the Burton lab (The Scripps Research Institute) for providing BA.2 and BA.4/5 gene fragments; and M. Cohen and J. Laux for assistance with cell sorting. We also thank N. Vaughan, K. Cooper, R. Reeder, M. St Claire, K. Hadley, D. Drawbaugh, A. Hischak, R. Hart, N. Isic, M. Murphy, E. Postnikova, M. Anantpadma, and E. Eudy for assistance with hamster experiments. We are grateful to the staff of Advanced Photon Source and Stanford Synchrotron Radiation Lightsource (SSRL) Beamline 12-1 for assistance with synchrotron data collection. **Funding:** This work was supported by the Division of Intramural Research and the Vaccine Research Center, National Institute of Allergy and Infectious Diseases (NIAID), National Institutes of Health (NIH) (L.D., S.M., J.W.Y., P.D.C., M.R.H., J.R.M., and J.T.). This project has been funded in whole or in part with federal funds from the NIAID, NIH, US Department of Health and Human Services (DHHS), under contract HHSN272201800013C. This work was also supported by NIH grant R01AI132317 (D.N. and L.P.), HHSN contract 75N93019C00073 (J.K.W. and E.D.), and Bill and Melinda Gates Foundation grant INV-004923 (I.A.W.). This research used resources of the Advanced Photon Source, a US Department of Energy (DOE) Office of Science user facility operated for the DOE Office of Science by Argonne National Laboratory under contract DE-AC02-06CH11357. GM/CA@APS has been funded by the National Cancer Institute (ACB-12002) and the National Institute of General Medical Sciences (AGM-12006 and P30GM138396). Extraordinary facility operations were supported in part by the DOE Office of Science through the National Virtual Biotechnology Laboratory, a consortium of DOE national laboratories focused on the response to COVID-19, with funding provided by the Coronavirus CARES Act. Use of the SSRL, SLAC National Accelerator Laboratory, is supported by the DOE, Office of Science, Office of Basic Energy Sciences, under contract DE-AC02-76SF00515. The SSRL Structural Molecular Biology

Program is supported by the DOE Office of Biological and Environmental Research and by the National Institute of General Medical Sciences of the NIH (P30GM133894). **Author contributions:** Conceptualization: J.T. and C.D. Methodology: C.D., C.T., L.Pe., C.-C.D.L., T.-H.L., M.Y., Y.C., L.W., D.D., B.E., I.K., Z.H., R.S.W., A.P., E.D., D.E.G., I.D., and S.M. Formal analysis: C.D., C.T., L.Pe., M.Y., Y.C., L.W., C.-C.D.L., T.-H.L., C.-W.P., J.S., and E.D. Data curation: M.P. Investigation: C.D., C.T., L.Pe., M.Y., L.W., C.-C.D.L., L.Pu., C.-W.P., J.K.W., T.-H.L., M.Z., M.P., D.M., A.J.R.C., S.D., E.K., L.H., D.P., R.B., S.L., D.D., B.E., Y.Z., E.S.Y., M.C., and K.L. Resources: R.S.W. and S.M. Writing – original draft: C.D., C.T., M.Y., and J.T. Writing – review & editing: all authors. Visualization: C.D., C.T., L.Pe., M.Y., Y.C., L.W., C.-C.D.L., J.K.W., E.D., and J.T. Supervision: E.D., D.E.G., S.M., J.W.Y., C.S., P.D.C., D.N., M.R.H., J.R.M., I.A.W., and J.T. Funding acquisition: C.S., P.D.C., D.N., M.R.H., J.R.M., I.A.W., and J.T. **Competing interests:** J.T. and C.D. are inventors on a provisional patent (US Patent Application no. 63/308,898) filed on the mAbs described in this study. J.K.W. and E.D. are employees of Integral Molecular. Y.C., S.D., E.K., L.H., D.P., R.B., S.L., D.D., B.E., and M.R.H. performed this work as employees of Laulima Government Solutions, LLC. The content of this publication does not necessarily reflect the views or policies of the DHHS or of the institutions and companies with which the authors are affiliated. All other authors declare no competing interests. **Data and materials availability:** All data associated with this manuscript are available in the main text or the supplementary materials. Crystal structures have been deposited into the Protein Data Bank (PDB IDs 8D36 for COV44-62, 8DAO for COV44-79, and 8D6Z for COV91-27). Antibody sequences have been deposited in GenBank (accession numbers ON695901 to ON695912). Materials described in this manuscript will be available through a material transfer agreement with the NIAID. **License information:** This work is licensed under a Creative Commons Attribution 4.0 International (CC BY 4.0) license, which permits unrestricted use, distribution, and reproduction in any medium, provided the original work is properly cited. To view a copy of this license, visit <https://creativecommons.org/licenses/by/4.0/>. This license does not apply to figures/photos/artwork or other content included in the article that is credited to a third party; obtain authorization from the rights holder before using such material.

SUPPLEMENTARY MATERIALS

[science.org/doi/10.1126/science.abq3773](https://doi.org/10.1126/science.abq3773)
Materials and Methods
Figs. S1 to S8
Tables S1 and S2
References (46–71)
MDAR Reproducibility Checklist

[View/request a protocol for this paper from Bio-protocol.](#)

Submitted 4 April 2022; accepted 6 July 2022
Published online 12 July 2022
[10.1126/science.abq3773](https://doi.org/10.1126/science.abq3773)

Broadly neutralizing antibodies target the coronavirus fusion peptide

Cherrelle DaconCourtney TuckerLinghang PengChang-Chun D. LeeTing-Hui LinMeng YuanYu CongLingshu WangLauren PurserJazmean K. WilliamsChul-Woo Pyolvan KosikZhe HuMing ZhaoDivya MohanAndrew J. R. CooperMary PetersonJeff SkinnerSaurabh DixitErin KollinsLouis HuzellaDonna PerryRussell ByrumSanae LembirikDavid DrawbaughBrett EatonYi ZhangEun Sung YangMan ChenKwanyee LeungRona S. WeinbergAmarendra PeguDaniel E. GeraghtyEdgar Davidsonlyadh DouagiSusan MoirJonathan W. YewdellConnie SchmaljohnPeter D. CromptonMichael R. HolbrookDavid NemazeeJohn R. Mascolalan A. WilsonJoshua Tan

Science, 377 (6607), • DOI: 10.1126/science.abq3773

Blocking a range of coronaviruses

Seven coronaviruses cause human disease, and three have caused serious outbreaks in the past 20 years. The potential for future coronavirus outbreaks in humans and the ongoing resistance of severe acute syndrome coronavirus 2 (SARS-CoV-2) variants to existing antibodies make it important to identify cross-reactive antibodies that can be the basis of therapeutics and can guide vaccine design. Low *et al.* and Dacon *et al.* isolated antibodies from convalescent individuals that show broad neutralizing activity against a range of coronaviruses, including Omicron variants of SARS-CoV-2. The antibodies target a conserved region of the viral spike protein known as the fusion peptide and may act by preventing the cell fusion that is required for infection of new host cells. —VV

View the article online

<https://www.science.org/doi/10.1126/science.abq3773>

Permissions

<https://www.science.org/help/reprints-and-permissions>

Use of this article is subject to the [Terms of service](#)

Science (ISSN) is published by the American Association for the Advancement of Science. 1200 New York Avenue NW, Washington, DC 20005. The title *Science* is a registered trademark of AAAS.

Copyright © 2022 The Authors, some rights reserved; exclusive licensee American Association for the Advancement of Science. No claim to original U.S. Government Works. Distributed under a Creative Commons Attribution License 4.0 (CC BY).